

## Article

# Solidification Segregation Behavior and Homogenization Process of a Difficult-to-Deform Superalloy Used at 850 °C

Wenbin Tai <sup>1,2</sup>, Rui Zhang <sup>1,\*</sup>, Chuanyong Cui <sup>1,\*</sup>, Zijian Zhou <sup>1</sup>, Yizhou Zhou <sup>1</sup> and Xiaofeng Sun <sup>1</sup>

<sup>1</sup> Shi-Changxu Innovation Center for Advanced Materials, Institute of Metal Research, Chinese Academy of Sciences, Shenyang 110016, China; wbtai@imr.ac.cn (W.T.)

<sup>2</sup> School of Materials Science and Engineering, University of Science and Technology of China, Shenyang 110016, China

\* Correspondence: rzhang@imr.ac.cn (R.Z.); chycui@imr.ac.cn (C.C.)

**Abstract:** Solidification segregation behavior and homogenization heat treatment processes of a difficult-to-deform superalloy for use at 850 °C were studied. Additionally, the effect of carbon content on homogenization, the thermal treatment process, and pore growth behavior within the alloy were discussed. Our results revealed that Al, Ti, and Nb elements are distributed in the interdendritic space, while W and Mo elements are distributed in the dendrite. There is a significant quantity of  $\gamma$ - $\gamma'$  eutectic and MC carbide precipitates in the interdendritic space. Notably, for the alloy containing 0.1 wt% C, a homogenization heat treatment at 1200 °C for 48 h can effectively eliminate the segregation and undesirable phases. As carbon content increased, the  $\gamma$ - $\gamma'$  eutectic phases diminished, and the homogenization time decreased accordingly. In this context, pores are smaller and more dispersed, which may enhance alloy forging properties.

**Keywords:** Ni-based superalloy; solidification segregation; homogenization heat treatment; pore growth behavior



**Citation:** Tai, W.; Zhang, R.; Cui, C.; Zhou, Z.; Zhou, Y.; Sun, X. Solidification Segregation Behavior and Homogenization Process of a Difficult-to-Deform Superalloy Used at 850 °C. *Crystals* **2023**, *13*, 1582. <https://doi.org/10.3390/cryst13111582>

Academic Editor: Andrei Vladimirovich Shevelkov

Received: 18 October 2023  
Revised: 3 November 2023  
Accepted: 8 November 2023  
Published: 14 November 2023



**Copyright:** © 2023 by the authors. Licensee MDPI, Basel, Switzerland. This article is an open access article distributed under the terms and conditions of the Creative Commons Attribution (CC BY) license (<https://creativecommons.org/licenses/by/4.0/>).

## 1. Introduction

The increasing thrust–weight ratio of aeroengines has placed great demands on temperature-bearing components, resulting in higher service temperatures for turbine disks [1–3]. The progression from the In718 alloy with a maximum temperature resistance of 650 °C, to the U720Li and TMW-4M3 alloys, capable of withstanding temperatures up to 700 °C, and ultimately to the ЭK151 alloy, renowned for its 800 °C resistance, reflects the evolving temperature capabilities of these materials [4–7]. The U720Li alloy has a strengthening phase element content of 7.5 wt%, while the ЭK151 alloy not only has a higher amount of strengthening phase elements (9.7 wt%), but also contains a solid solution element content as high as 33.5 wt%. With improved thermal strength comes higher levels of alloying, leading to significant solidification segregation and eutectic precipitation during smelting, posing challenges for subsequent alloy forging [8]. Consequently, it is crucial to investigate solidification segregation behavior and homogenization heat treatment processes for such alloys. The investigation of the solidification segregation behavior of alloys may reveal an understanding of the fundamental connection between chemical composition and microstructure. By controlling the chemical composition, the homogeneity of the alloy structure can be improved in a more effective way. The research on homogenization heat treatment technique aims to achieve cost-effective and efficient alloy homogenization, thereby ensuring optimal forging performance.

Homogenization heat treatment has been intensively researched as an effective method for solidification segregation in as-cast superalloys. Zhou et al. [9] conducted an analysis of homogenization heat treatments for directionally solidified Ni–Co-based alloys, and developed a kinetic diffusion model for element migration. Semiatin et al. [10,11] investigated the homogenization kinetics of Waspaloy alloys using a simple diffusion model. The

engineering interdiffusion coefficients of Ti, Co, and Cr elements were calculated by the Ni–X binary alloy.

This study focuses on a nickel-based superalloy designed for operation at 850 °C, featuring a significant presence of precipitate and solution strengthening elements, as well as a C content ranging from 0.1 to 0.15 wt%. Carbon, as the primary constituent of carbide, has been the subject of prolonged research, with a specific focus on its influence on the microstructure of superalloys. The addition of C has been demonstrated to effectively purify alloys and improve their performance [12,13]. However, an excessive presence of carbide was reported to promote the propagation of surface cracks [13,14]. To date, investigations into the impact of C on the microstructure of wrought superalloys have primarily centered on alloys with low C content (not exceeding 0.05 wt%) and low concentrations of strengthening phase elements. The effects of higher C content on the microstructure of these high-temperature-resistant alloys remain largely unexplored. In this experiment, we investigated the segregation behavior and the influence of varying C content on the segregation process, including the examination of the segregation coefficient of elements at different positions, and the determination of the area fraction of precipitated phases. Furthermore, we explore the homogenization behavior of the alloy with different C contents, and develop an optimized homogenization thermal treatment process.

## 2. Materials and Methods

Three alloys with different C contents were prepared using a vacuum induction furnace, with their nominal compositions listed in Table 1. The accuracy of alloy composition was ensured by a spectrometer and a C/S tester. The diameter of the obtained rods is approximately 80 mm. Microstructure observations were conducted on samples taken from the center of the ingot. In order to eliminate element segregation and harmful phases in the alloys, the homogenization behavior of alloys with the proper chemical composition was studied. Homogenization heat treatment was carried out at various temperatures for the 0.1% C alloy samples. The specimens underwent homogenization for 6 h at 1180, 1190, 1200, and 1210 °C to assess the microstructure evolution. Homogenization heat treatment was also applied to both 0.1% C and 0.15% C alloys at 1200 °C for durations of 3, 6, 12, 24, and 48 h with water cooling.

**Table 1.** Chemical composition of alloy ingot with different C contents (wt%).

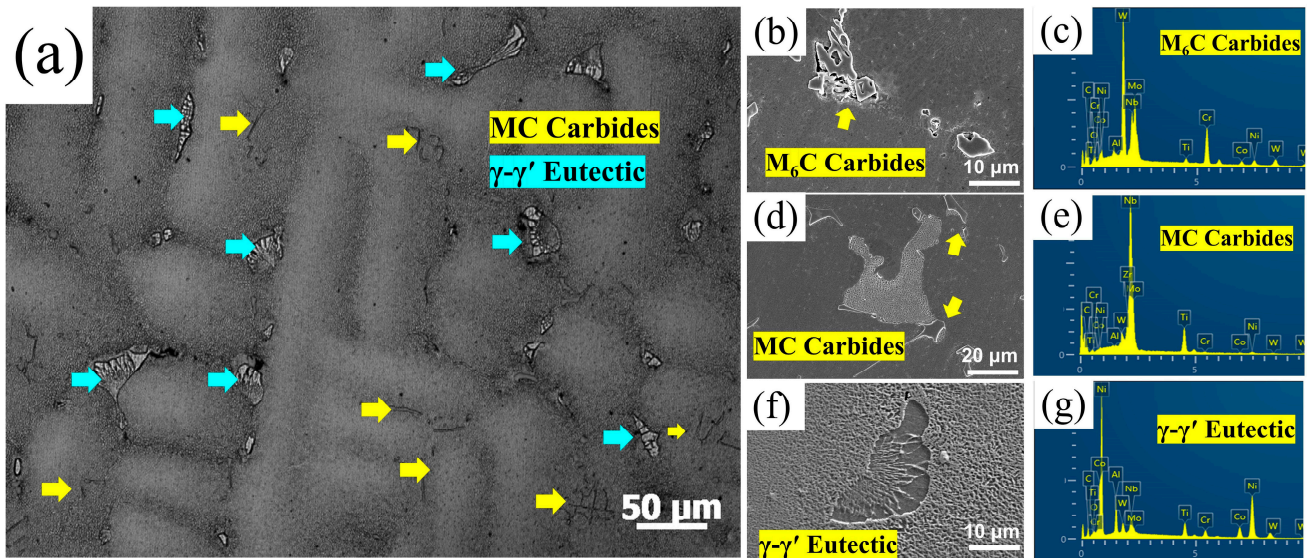
C	Cr	Co	Al + Ti + Nb	W + Mo	B + Zr	Ni
0.05						
0.1	8	15–18	9–10	10–13	0.02–0.1	Bal.
0.15						

For metallographic observation, specimens were mechanically ground, polished to a mirror surface, and chemically etched for 10 s at room temperature using a solution of ethanol (100 mL) + HCl (100 mL) + CuCl<sub>2</sub> (50 g). Dendrites and precipitates were characterized using optical microscopy (OM) (Zeiss, Shanghai, China) and scanning electron microscopy (SEM) (Tescan, Brno, Czech Republic). Element segregation was analyzed by electron probe X-ray microanalyzer (EPMA) (Shimadzu, Tokyo, Japan) and scanning electron microscopy energy dispersive spectrometer (SEM-EDS) (Tescan, Brno, Czech Republic).

## 3. Results

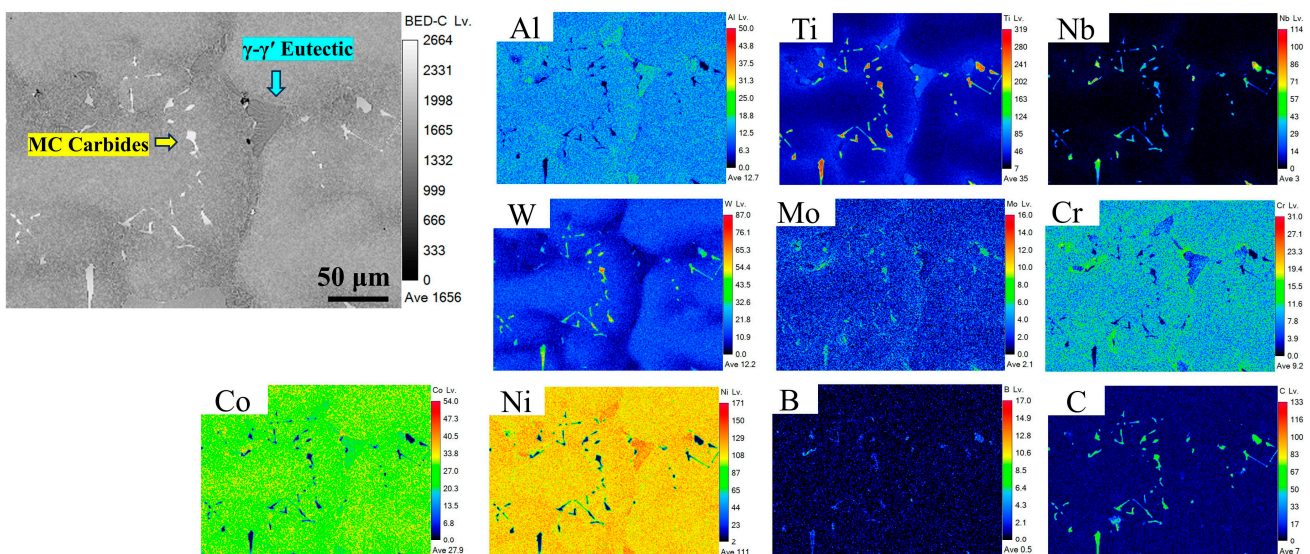
### 3.1. As-Cast Microstructure and Solidification Segregation Behavior of Alloy

Figure 1 illustrates OM and SEM images of the microstructure in the center of a 0.1 wt% C alloy ingot. The alloy exhibits a distinct dendrite morphology, with numerous  $\gamma$ - $\gamma'$  eutectic precipitates and carbides in the interdendritic region. Compositional analysis by SEM-EDS reveals that these carbides consist of MC and M<sub>6</sub>C carbides.



**Figure 1.** Microstructure analysis of the as-cast 0.1 wt% C alloy: (a) microstructure pictures using OM, (b) SEM image of  $M_6C$ , (c) SEM-EDS analysis of  $M_6C$  carbides, (d) SEM image of MC carbides, (e) SEM-EDS analysis of MC carbides, (f) SEM image of  $\gamma$ - $\gamma'$  eutectic phases, (g) SEM-EDS analysis of  $\gamma$ - $\gamma'$  eutectic phases.

The EPMA results in Figure 2 show varying levels of element segregation between interdendritic and dendritic regions. The precipitate phases are marked differently in the figure. Al, Ti, and Nb tend to concentrate within the interdendritic regions, while Co, Cr, and Mo exhibit a more uniform dispersion throughout the alloy. A notable amount of W exhibits segregation in the dendritic area. Furthermore, it is seen that the  $\gamma$ - $\gamma'$  eutectic phases exhibit enrichment of Al, Ti, and Ni, with a depletion of Co, Cr, and W. Additionally, a Cr-rich band is also observed at the outer edge of these phases. The primary constituents of MC carbides are (Nb, Ti, W, Mo)C, and it can be found that B elements are concentrated in MC carbides. In addition, through the observation of the microstructure and investigation of related studies [1,14], we also confirmed that there is no boride precipitation in the alloy.



**Figure 2.** Distribution map of elements in the as-cast alloy with 0.1 wt% C.

The as-cast microstructure of the alloy exhibits significant element segregation and the presence of precipitated phases, attributed to variations in elemental diffusion rates [15–19]. Elements possessing high diffusion coefficients, such as Al and Ti, have a propensity to segregate towards interdendritic regions during solidification. Conversely, W, Mo, and other elements with slower diffusion rates aggregate at dendritic regions. Elements with moderate diffusion rates are uniformly distributed within the microstructures. In this experimental alloy, a significant quantity of strengthening elements, namely Al, Ti, and Nb, exhibit segregation inside interdendritic regions, along with the presence of many MC carbides and eutectic structures. As a grain boundary strengthening element, C is more likely to segregate at grain boundaries, but for as-cast alloys with large grain sizes, a large amount of C is also distributed in grains [20,21]. During solidification, Ti and Nb elements segregate to the interdendritic area due to their fast diffusion rates, and then combine with the C element to form a large number of carbides. It should be noted that the W element is also the MC carbide-forming element in the alloys studied in this experiment, which leads to the MC carbide precipitation position not being completely in the interdendritic area. Cr, with a moderate diffusion rate, does not lead to apparent segregation. However, due to the formation of large-sized  $\gamma$ - $\gamma'$  eutectic phases without Cr, the Cr element remains in its original position without sufficient time for even diffusion into the structure. As a consequence, Cr-rich regions develop around the  $\gamma$ - $\gamma'$  eutectic structures. This phenomenon aligns with the findings of a study conducted by Li et al. [22]. In contrast to other difficult-to-deform superalloys, such as  $\text{XK151}$  and  $\text{TMW-4M3}$ , despite the substantial content of strengthening phase elements, the  $\eta$  phase is not observed in the microstructure of this alloy. This could be attributed to the alloy's Ti/Al ratio, which is approximately 0.5. It is worth noting that when the Ti/Al ratio in an alloy exceeds 1.6, there is a greater tendency for the precipitation of the  $\eta$  phase [23].

### 3.2. Microstructure and Element Segregation of Alloys with Different C Contents

The microstructures of alloys with varying carbon concentrations are displayed in Figure 3. The precipitated phases in the figure are marked with different colors. These alloys exhibit a distinct dendritic morphology, with the presence of  $\gamma$ - $\gamma'$  eutectic phases and carbides inside the interdendritic regions. As shown in Figure 3, in the alloy with a C content of 0.05 wt%, a significant number of large-sized  $\gamma$ - $\gamma'$  eutectic phases are observed, along with microcracks (represented by red arrow) propagating along these large eutectic phases. Additionally, only a small quantity of massive carbides is observed at this point. As the C content increases, both the size and quantity of the  $\gamma$ - $\gamma'$  eutectic phases decrease noticeably, while the precipitation of carbides increases significantly. Furthermore, the carbide morphology transforms from block-like to strip-like and skeletal. The dendrite spacing of the alloy was calculated, and the results are presented in Figure 4a. The research findings indicate that the increase in carbon content has no impact on the distance between dendrites in the alloy. Studies have indicated that the dendrite spacing in an alloy can influence its homogenization behavior. Furthermore, the area fraction of  $\gamma$ - $\gamma'$  eutectic and MC carbides in the microstructure of the as-cast alloy with different C contents has been subjected to statistical analysis, and the statistical results are displayed in Figure 4b.

The results reveal a positive correlation between carbon content and the area fraction of carbides in the as-cast alloy, while conversely, there is a negative relationship between the carbon content and the area fraction of eutectic phases. Several studies have demonstrated that the element C, as a grain boundary strengthening agent, enhances the bonding force in alloys through two mechanisms [24–28]. Firstly, C segregates at grain boundaries, thereby reinforcing the bonding force. Secondly, C forms carbides that act as pinning agents, further reinforcing the grain boundaries and strengthening the overall alloy. For the as-cast microstructure of wrought superalloys, the effect of C on the alloy is mainly concentrated on the segregation of elements and the area fraction of precipitated phases.

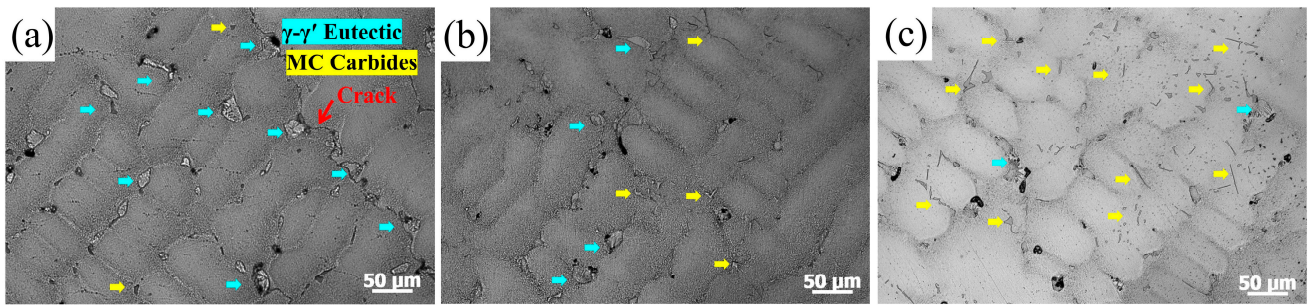


**Figure 3.** As-cast microstructure of alloys with different C contents: (a) 0.05 wt%, (b) 0.1 wt%, and (c) 0.15 wt%.

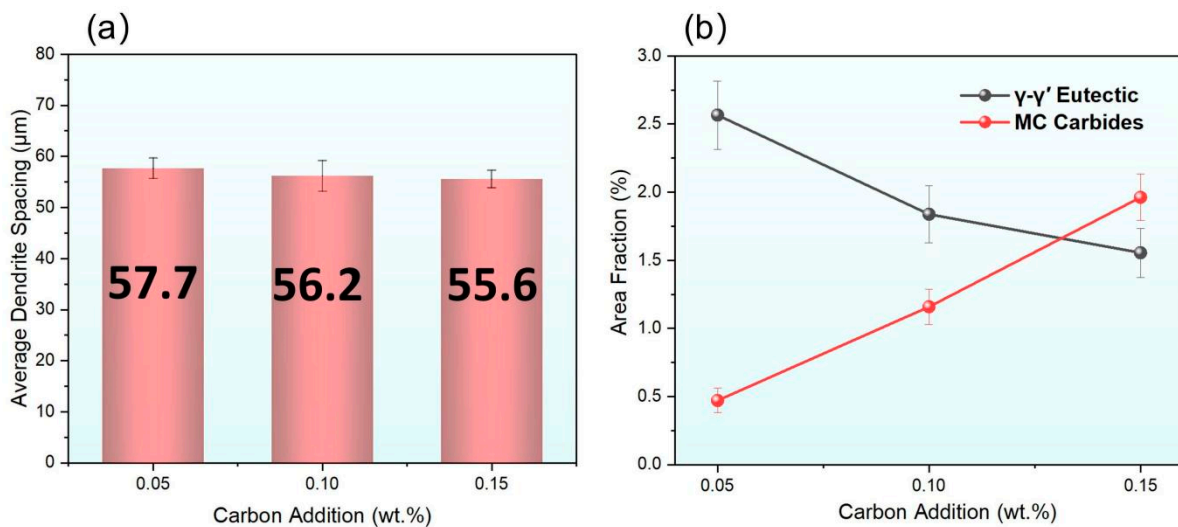


**Figure 4.** (a) The dendrite spacing and (b) the area fraction of precipitated phases in as-cast alloys with different C contents.

The beneficial impact of carbon (C) on alloy purification has been observed in some difficult-to-deform superalloys [29–31]. Numerous studies have demonstrated that during the cooling process of liquid superalloys, the MC phase precipitates from the matrix prior to the  $\gamma$ - $\gamma'$  eutectic phase due to its higher melting point. This precipitation of MC carbide consumes some of the elements required for  $\gamma$ - $\gamma'$  eutectic phase formation, thereby reducing its formation [20,32,33]. In our studied alloys, the EPMA results clearly show the presence of significant amounts of Ti and Nb elements in both the  $\gamma$ - $\gamma'$  eutectic and MC carbides. When the C content increases, more Nb and Ti elements in the alloy combine with carbon to form additional MC carbides. Consequently, the density of elements required for the  $\gamma$ - $\gamma'$  eutectic phase decreases, reducing the tendency for  $\gamma$ - $\gamma'$  eutectic phase precipitation. This relationship is illustrated in Figure 4b, where a decrease in the  $\gamma$ - $\gamma'$  eutectic phase coincides with an increase in MC carbides. Consequently, there is a reduction in the presence of  $\gamma$ - $\gamma'$  eutectic phases [29]. Additionally, some studies have suggested that during the solidification of the alloy, a significant amount of precipitated carbides occupies the position where  $\gamma$ - $\gamma'$  eutectic phases would normally form within the liquid pool [31]. This phenomenon contributes to a reduced precipitation of the  $\gamma$ - $\gamma'$  eutectic phases. Notably, unlike other difficult-to-deform superalloys such as U720Li, the as-cast structure of the alloy still contains a certain quantity of  $\gamma$ - $\gamma'$  eutectic phases, even with an increase in C content up to 0.15 wt%. This observation may be attributed to the high Al content in the alloy. The increase in C content has a minimal impact on the distribution of Al elements, and the segregation of Al elements makes it challenging to entirely eliminate the  $\gamma$ - $\gamma'$  eutectic phases in the as-cast structure of the alloy.

Statistical analysis of dendrite segregation of alloy elements was carried out using SEM-EDS to investigate the influence of C content on the extent of alloy element segregation, and the results are presented in Figure 5. Solute segregation within the alloy can be characterized by the microsegregation coefficient, which can be quantitatively described by the following formula [34]:

$$K = \frac{C_S}{C_L} \quad (1)$$

Here,  $K$  represents the microsegregation coefficient of an element, with  $C_S$  and  $C_L$  denoting the concentration of an element in the dendritic and interdendritic regions, respectively. As illustrated in Figure 5, Al, Ti, and Nb all exhibit  $K$  values less than 1, indicating that they are negative segregation elements. Conversely, Cr, Co, and W are positive segregation elements, consistent with the finding discussed in Section 3.1. Generally, in the as-cast microstructure of superalloys, element content, cooling rate, dendrite spacing, and alloying element systems also affect element segregation and homogenization behavior [10,11,35,36]. However, in the alloys we have studied, the cooling rate, dendrite spacing, and elemental system of the alloy have no obvious differences. Therefore, the segregation behavior of the alloy is mainly affected by the change in C content. The microstructure of the alloy and the degree of element segregation within the dendrite both undergo changes as the C concentration increases. In line with S. Tin and T.M. Pollock's analysis of a single crystal superalloy [21], the segregation of elements such as W, Ta, and Re is less pronounced in alloys containing C compared to those without C. Furthermore, as suggested by Xu's research [31], C can influence the degree of segregation of the Ta and W components. Notably, among the alloy components, carbon concentration has the most significant impact on the segregation of W. Unlike other alloys, the carbides in this alloy are not only rich in Ti and Nb, but also in W. With an increase in C concentration, Ti, Nb, and W are utilized more in the formation of MC carbides. As the area fraction of  $\gamma$ - $\gamma'$  eutectic phases decreases in the alloy due to the reduction in Ti and Nb elements, the segregation of these components has minimal influence. However, the formation of carbides consumes a significant amount of W within the interdendritic regions, and given the low W element diffusion coefficient [18,19], this further exacerbates the segregation of W elements.

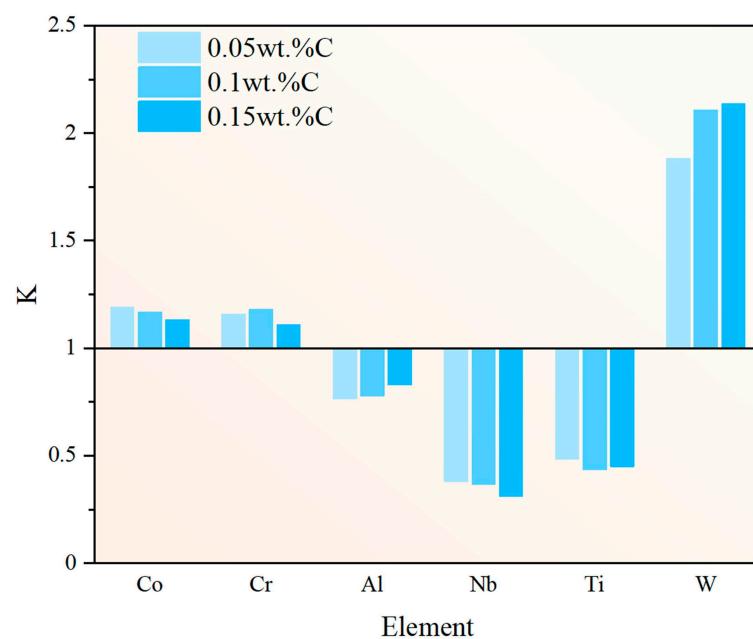


Figure 5. Effect of C content on segregation of alloying elements.

### 3.3. Effect of Homogenization Heat Treatment on Microstructure

The alloy we studied, known for its challenging deformability, exhibits a substantial presence of  $\gamma$ - $\gamma'$  eutectic phases and carbides in its as-cast microstructure. MC carbides and  $\gamma$ - $\gamma'$  eutectic phases are common brittle phases in superalloys [13,37]. The  $\gamma$ - $\gamma'$  eutectic phases with large sizes are easier to crack and form crack sources during forging deformation due to their limited plasticity. The cracks propagate or combine into larger cracks in subsequent deformation, resulting in the failure of the alloy. Furthermore, the pronounced segregation of strengthening elements within the alloy makes it vulnerable to the initiation of forging fractures, thereby adversely affecting its overall forging performance [9]. To reduce element segregation and brittle  $\gamma$ - $\gamma'$  eutectic phases, and to enhance the alloy's forging characteristics, the implementation of an efficient homogenization heat treatment method has become imperative. Based on the findings from Sections 3.1 and 3.2, we have determined that decreasing the C content leads to the precipitation of larger eutectic phases, which are prone to crack initiation. Consequently, 0.1 wt% C and 0.15 wt% C alloys with higher engineering values were selected for further homogenization studies.

#### 3.3.1. Effect of Homogenization Heat Treatment Temperature on Microstructure

In order to determine the optimum homogenization heat treatment temperature of the alloy more accurately, a 0.1 wt% C alloy was used for experiments for its more harmful  $\gamma$ - $\gamma'$  eutectic phases with large size. The as-cast alloy underwent a homogenization process at temperatures of 1180 °C, 1190 °C, 1200 °C, and 1210 °C, each lasting for 6 h. Water cooling was employed as the cooling method to facilitate a more direct observation of the microstructure changes resulting from various homogenization heat treatments. The alloy microstructure after different homogenization heat treatment conditions is shown in Figure 6. At heat treatment temperatures of 1180 °C and 1190 °C (depicted in Figure 6a,b), improvements in element segregation within the alloy are observed. Nevertheless, the alloy retains a complete dendrite morphology and eutectic structure due to the relatively low temperature and the slow movement of elements. Upon reaching a heat treatment temperature of 1200 °C (Figure 6c), an accelerated rate of element diffusion is noted, leading to a significant reduction in element segregation within the alloy. Moreover, to some extent, the microstructure exhibits a dissolution of carbides and  $\gamma$ - $\gamma'$  eutectic phases. As depicted in Figure 6d, when the heat treatment temperature is further raised to 1210 °C, the alloy's dendritic element segregation is effectively eliminated, and both the  $\gamma$ - $\gamma'$  eutectic phases and carbides are essentially redissolved. However, it should be noted that certain  $\gamma$ - $\gamma'$  eutectic phases with lower melting points exhibit some premature melting due to the elevated heat treatment temperature; the incipient melting structures are shown in Figure 6d. Only carbides and  $\gamma$ - $\gamma'$  eutectic phases remain in the cast microstructure. Since the melting point of MC carbides is typically higher, the presence of a substantial quantity of  $\gamma$ - $\gamma'$  eutectic phases lowers the initial melting temperature of the alloy [33,37]. This, in turn, increases the susceptibility of the alloy to crack formation during the solidification of the initial melting structure. These factors have a significant impact on the forging properties of the alloy. Therefore, it is advisable to limit the homogenization temperature of the alloy to a maximum of 1200 °C.

#### 3.3.2. Effect of Homogenization Heat Treatment Time on Microstructure

Based on the research findings presented in Section 3.3.1, a homogenization heat treatment temperature of 1200 °C was selected for the alloy. This temperature was chosen to investigate the relationship between element segregation and microstructure in alloys with varying carbon contents and different processing times. Figure 7 provides a visual representation of the microstructural changes in 0.1 wt% C and 0.15 wt% C alloys following 3 h, 24 h, and 48 h of homogenization heat treatment. The  $\gamma$ - $\gamma'$  eutectic phases and pores of different sizes are marked by different colored arrows. As seen in Figure 7a,d, after just 3 h of homogenization heat treatment, the segregation in alloys with different carbon contents is significantly reduced, and the dendritic structure is largely retained in the alloy. However, during this phase, a few micropores begin to appear amidst the interdendritic area of the

alloy. Upon extending the homogenization heat treatment to 24 h, a notable improvement in the segregation of components, including  $\gamma$ - $\gamma'$  eutectic phases and MC carbides, is observed in the 0.15 wt% C alloy, accompanied by the development of a substantial number of scattered pores (Figure 7e). In contrast, even though the segregation of elements in the 0.1 wt% C alloy is greatly improved after 24 h (Figure 7b), the alloy still contains a small quantity of MC carbides and some  $\gamma$ - $\gamma'$  eutectic phases. As the duration of the heat treatment is further extended to 48 h (Figure 7c,f), it becomes evident that both alloys undergo complete elimination of segregation and detrimental phases. Notably, the average pore diameter in the alloy increases to approximately 10  $\mu\text{m}$  during this extended treatment period.

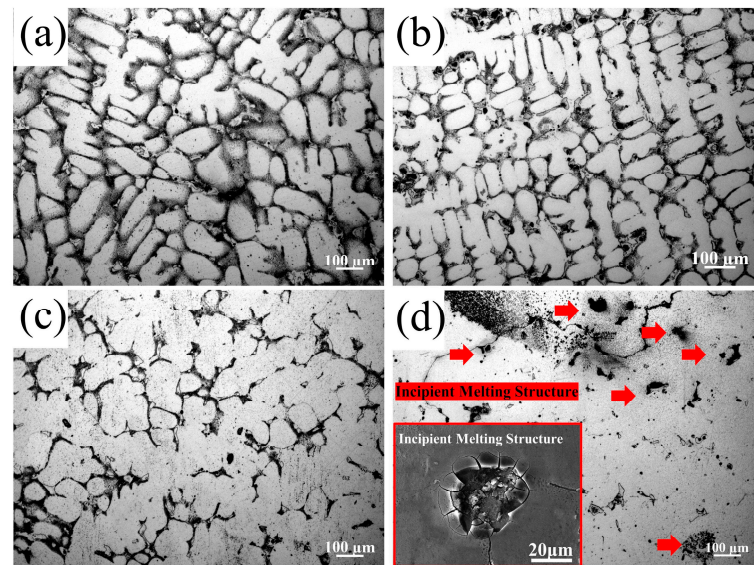


**Figure 6.** Microstructure of alloy after homogenization heat treatment at different temperatures: (a) 1180 °C, (b) 1190 °C, (c) 1200 °C, and (d) 1210 °C and incipient melting structures in alloy.

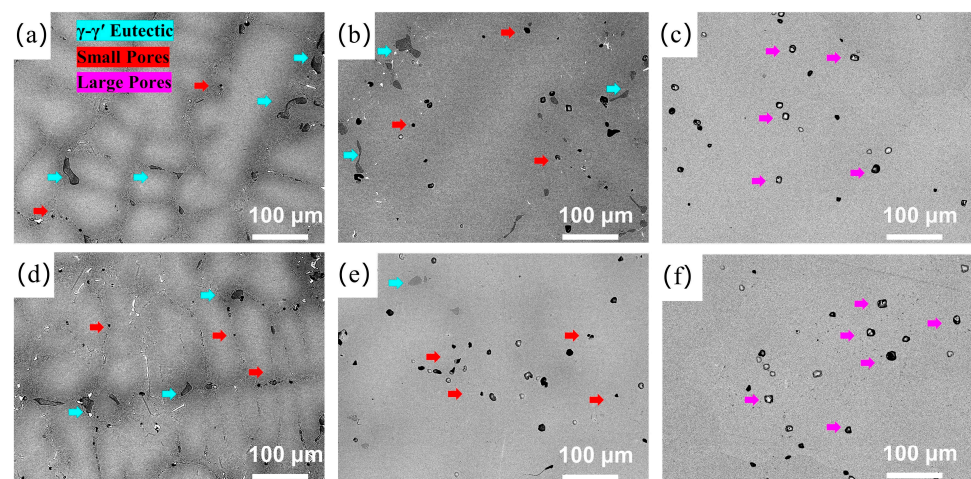


**Figure 7.** Microstructure of alloy: with (a–c) 0.1 wt% C and (d–f) 0.15 wt% C; after homogenization heat treatment for different times: (a,c) 3 h, (b,e) 24 h, and (c,f) 48 h.

The area surrounding the pores in the alloy was carefully examined through SEM-EDS analysis. Different precipitated phases can be effectively distinguished by component testing, and the results are illustrated in Figure 8. It is evident that the huge bulk phases next to the pore are abundant with the elements Ni and Al, indicating that they are  $\gamma$ - $\gamma'$  eutectic phases. Additionally, it is possible to identify MC carbides as the tiny bulk phases that are abundant in Ti, Nb, and other elements. It shows that the pores with smooth edge

morphology grow near the  $\gamma$ - $\gamma'$  eutectic phases and MC carbides. In addition, incomplete redissolved MC carbides were observed in the lower left corner of the pores.

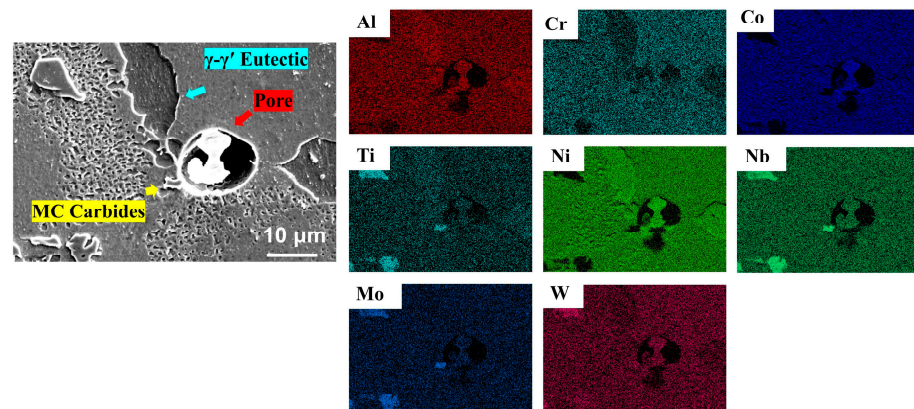


**Figure 8.** Distribution map of elements in the area around the pore formed by homogenization heat treatment.

The results of the statistical analysis on the degree of dendrite segregation of alloys with various C contents at 1200 °C and various homogenization times are depicted in Figure 9. It can be seen from the figure that the distribution of each element within the alloy approaches equilibrium after approximately 35 h for the 0.1 wt% C alloy, whereas the alloy with a 0.15 wt% C content achieves this equilibrium in approximately 25 h. This suggests that a higher carbon concentration in the alloy may expedite the homogenization of the microstructure.

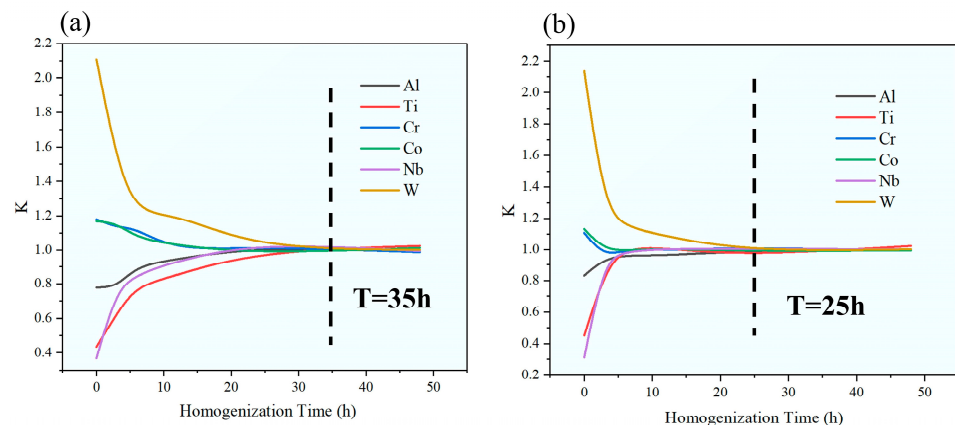


**Figure 9.** Homogenization time dependence of dendrite segregation in alloys with different C contents: (a) 0.1 wt% C, and (b) 0.15 wt% C.

## 4. Discussion

### 4.1. Pore Growth Mechanism

Numerous studies indicate that the Kirkendall effect is the primary cause of the emergence of pores in alloys [19,33,38,39]. This phenomenon arises due to the differential rates at which elements move within alloys. Atoms with higher mobility generate vacancies that are not promptly filled by atoms with slower mobility, resulting in the accumulation of vacancies and the subsequent formation of pores. Additionally, other research has contributed supplementary explanations for the genesis of pores. For example, Alexander et al. [38] conducted a study on a single crystal superalloy and revealed that pore expansion can also be triggered by the disintegration of the eutectic structure and changes in the alloy's volume induced by heat treatment. D.L. Anton's research further demonstrated

that alloys can lead to void expansion due to alterations in molar volume during phase transitions [39].

In our experimental alloys, the primary sites of pore growth were found to be in proximity to the  $\gamma$ - $\gamma'$  eutectic phases and carbides, implying that most voids are created through the solid solution process involving these components. During the homogenization process,  $\gamma$ - $\gamma'$  eutectic phases and carbides dissolve back into the matrix, resulting in the formation of micropores near their original locations. This is driven by the Kirkendall effect and molar volume changes during phase transformations. With increased homogenization time, elements become more uniformly distributed throughout the alloy. Interdendritic segregation elements such as Al, Ti, and Nb migrate toward the dendrites, while elements such as W and Mo, involved in dendritic segregation, move at a slower pace and have difficulty filling the voids left by other elements. Consequently, a substantial accumulation of vacancies occurs, leading to the formation and subsequent expansion of micropores. The EDS analysis also revealed the persistence of partially dissolved MC carbides and  $\gamma$ - $\gamma'$  eutectic phases in close proximity to these pores.

#### 4.2. Homogenization Behavior of Alloys with Different C Contents

During the alloy's homogenization process, it is worth noting that the redissolution temperature of  $\gamma$ - $\gamma'$  eutectic phases is lower than that of carbides, making them more prone to redissolving into the alloy matrix, and thus contributing to the formation of pores. However, in the case of this particular alloy, which contains a substantial quantity of strengthening phase elements, a significant proportion of  $\gamma$ - $\gamma'$  eutectic phases is present in the as-cast structure. To effectively homogenize this alloy, a high temperature of up to 1200 °C is employed, which accelerates the movement of elements. At this elevated temperature, MC carbides exhibit a slightly higher redissolution temperature compared to  $\gamma$ - $\gamma'$  eutectic phases. Nevertheless, due to the presence of numerous large  $\gamma$ - $\gamma'$  eutectic phases, which are significantly larger in size than MC carbides, a prolonged period is often required for them to fully redissolve. Consequently, this extended time frame leads to the retention of a substantial number of larger pores within the alloy.

Previous research has provided evidence that both the area fraction and size of  $\gamma$ - $\gamma'$  eutectic phases decrease as the C content increases [40]. Smaller and more evenly distributed  $\gamma$ - $\gamma'$  eutectic phases are more readily redissolved during the alloy's homogenization process. The dissolution rate of undesirable phases during the homogenization of 0.15 wt% C alloys is accelerated, resulting in a superior homogenization effect for precipitated phases compared to 0.1 wt% C alloys processed for the same duration. As depicted in Figure 9, alloys containing 0.15 wt% C content achieve element homogenization in approximately 24 h, whereas alloys with 0.1 wt% C content require a longer duration. This difference can be attributed to the significant consumption of Ti and Nb elements by the MC carbides in the alloy. Despite having a limited impact on their segregation ratios in the alloy, the reduced dispersion of Ti and Nb elements in the alloy facilitates reaching the homogenization stage sooner. Furthermore, a lower percentage of  $\gamma$ - $\gamma'$  eutectic phase area allows Cr, Co, and other elements with moderate diffusion rates to distribute more rapidly and uniformly throughout the alloy. Additionally, certain W and Mo elements become enriched in the carbides of the experimental alloys. The dissolution of carbides expedites the movement of W and Mo elements, which have lower diffusion rates, toward the dendrites, further accelerating the homogenization process of the alloys to a certain extent.

Pores resulting from the dissolution of MC carbides are smaller in size compared to those formed through the resolution of the eutectic structure. This discrepancy arises from the substantial difference in average size between MC carbides and the eutectic structure during the homogenization process. Consequently, the C content also exerts an influence on the alloy's homogenization behavior. The progression of the homogenization process over time for various C contents is illustrated in Figure 10. In low carbon alloys, the microstructure consists of numerous  $\gamma$ - $\gamma'$  eutectic phases and tiny MC carbides. These small MC carbides gradually dissolve, generating smaller pores during homogenization.

Coarse  $\gamma$ - $\gamma'$  eutectic phases exhibit a faster dissolution rate, but their larger size prolongs the dissolution process. As time advances, all the large  $\gamma$ - $\gamma'$  eutectic phases dissolve back into the matrix, giving rise to larger pores, while the smaller pores formed earlier tend to aggregate and grow. Conversely, in high-carbon alloys, fewer and smaller  $\gamma$ - $\gamma'$  eutectic phases precipitate as the carbide content increases. The dissolved MC carbides form dispersed small pores, and the  $\gamma$ - $\gamma'$  eutectic phases also dissolve to create smaller pores. At this stage, the detrimental phases have dissolved back into the alloy, resulting in a homogenized structure characterized by smaller and more evenly distributed pores. Over time, these small pores tend to aggregate, forming larger pores. It is worth noting that significant cavities can adversely affect the properties of an alloy [37,41].

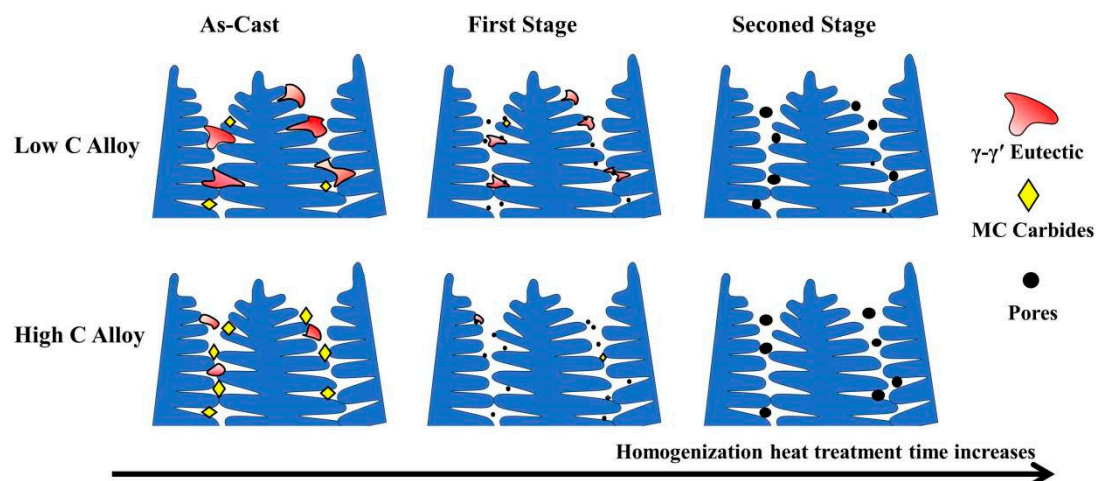


**Figure 10.** Schematic diagram of hole growth during the homogenization treatment.

## 5. Conclusions

The study of solidification segregation behavior and homogenization process of a hard-to-deform nickel-base superalloy used at 850 °C can be described as follows:

1. The alloy displays a clear dendritic distribution in its as-cast microstructure. Among the interdendritic regions, elements such as Al, Ti, and Nb are dispersed, while W and Mo elements are distributed within the dendrites. Additionally, numerous  $\gamma$ - $\gamma'$  eutectic phases and MC carbides are precipitated among the interdendritic regions.
2. An increase in C content leads to a reduction in the presence of  $\gamma$ - $\gamma'$  eutectic phases in the as-cast alloy. This reduction may have a favorable impact on the forging performance of the alloy.
3. In the case of the alloy containing 0.1 wt% C, effective elimination of element segregation and  $\gamma$ - $\gamma'$  eutectic phases can be achieved through homogenization heat treatment at 1200 °C for 48 h.
4. The time required for the homogenization heat treatment can be appropriately decreased with an increase in C content. Consequently, smaller and more uniformly distributed pores are observed, which can contribute to the improved forging characteristics of the alloy.

**Author Contributions:** Conceptualization, W.T. and R.Z.; methodology, W.T.; software, Z.Z.; validation, W.T., R.Z. and Z.Z.; formal analysis, C.C.; investigation, W.T.; resources, Y.Z.; data curation, W.T.; writing—original draft preparation, W.T.; writing—review and editing, R.Z.; visualization, W.T.; supervision, X.S.; project administration, C.C.; funding acquisition, Y.Z. All authors have read and agreed to the published version of the manuscript.

**Funding:** This research was funded by the National Science and Technology Major Project (J2019-VI-0006-0120), the National Key R&D Program of China (No. 2019YFA0705300), the Natural Science Foundation Project of Liaoning Province (No. 2023-MS-024), and the Youth Innovation Promotion Association, CAS (No. 2023202).

**Data Availability Statement:** The data presented in this study are available in the article.

**Conflicts of Interest:** The authors declare no conflict of interest.

## References

1. Wang, Y.; Tan, Y.; Li, X.; You, X.; Zhao, J.; Li, M.; Bai, R.; Li, P. Microstructures and homogenization behavior of a nickel-based superalloy used for 850 °C turbine disc prepared by electron beam smelting layered solidification. *J. Alloys Compd.* **2023**, *935*, 168119. [\[CrossRef\]](#)
2. Logunov, A.V.; Zavodov, S.A.; Danilov, D.V. The Challenges in Development of Nickel-Based Heat-Resistant Superalloys for Gas Turbine Disks and Creation of a New Superalloy with Increased Operational Characteristics. *Mater. Today Proc.* **2019**, *11*, 459–464. [\[CrossRef\]](#)
3. Henderson, M.B.; Arrell, D.; Larsson, R.; Heobel, M.; Marchant, G. Nickel based superalloy welding practices for industrial gas turbine applications. *Sci. Technol. Weld. Join.* **2004**, *9*, 13–21. [\[CrossRef\]](#)
4. Zhang, J.; Wu, C.; Peng, Y.; Xia, X.; Li, J.; Ding, J.; Liu, C.; Chen, X.; Dong, J.; Liu, Y. Hot compression deformation behavior and processing maps of ATI 718Plus superalloy. *J. Alloys Compd.* **2020**, *835*, 155195. [\[CrossRef\]](#)
5. Chang, L.; Jin, H.; Sun, W. Solidification behavior of Ni-base superalloy Udimet 720Li. *J. Alloys Compd.* **2015**, *653*, 266–270. [\[CrossRef\]](#)
6. Yuan, Y.; Gu, Y.; Osada, T.; Zhong, Z.; Yokokawa, T.; Harada, H. Deformation mechanisms in a new disc superalloy at low and intermediate temperatures. *Scr. Mater.* **2012**, *67*, 137–140. [\[CrossRef\]](#)
7. Xinxu, L.; Chonglin, J.; Yong, Z.; Shaomin, L.; Zhouhua, J. Segregation and homogenization for a new nickel-based superalloy. *Vacuum* **2020**, *177*, 109379. [\[CrossRef\]](#)
8. Li, Y.; Dong, Y.; Jiang, Z.; Yao, K.; Du, S.; Liu, Y.; Hou, Z. Study on microsegregation and homogenization process of a novel nickel-based wrought superalloy. *J. Mater. Res. Technol.* **2022**, *19*, 3366–3379. [\[CrossRef\]](#)
9. Zhou, Z.; Zhang, R.; Cui, C.; Zhou, Y.; Sun, X. Effects of Homogenization Treatment on the Microsegregation of a Ni-Co Based Superalloy Produced by Directional Solidification. *Acta Metall. Sin.* **2021**, *34*, 943–954. [\[CrossRef\]](#)
10. Semiatin, S.; Kramb, R.; Turner, R.; Zhang, F.; Antony, M. Analysis of the homogenization of a nickel-base superalloy. *Scr. Mater.* **2004**, *51*, 491–495. [\[CrossRef\]](#)
11. Kramb, R.; Antony, M.; Semiatin, S. Homogenization of a nickel-base superalloy ingot material. *Scr. Mater.* **2006**, *54*, 1645–1649. [\[CrossRef\]](#)
12. Wei, C.-N.; Bor, H.-Y.; Chang, L. The influence of carbon addition on carbide characteristics and mechanical properties of CM-681LC superalloy using fine-grain process. *J. Alloys Compd.* **2011**, *509*, 5708–5714. [\[CrossRef\]](#)
13. Al-Jarba, K.; Fuchs, G. Effect of carbon additions on the as-cast microstructure and defect formation of a single crystal Ni-based superalloy. *Mater. Sci. Eng. A* **2004**, *373*, 255–267. [\[CrossRef\]](#)
14. Jiang, H.; Xiang, X.; Dong, J. The morphology and characteristics evolution of MC carbide during homogenization in hard-to-deform superalloy GH4975. *J. Alloys Compd.* **2022**, *929*, 167086. [\[CrossRef\]](#)
15. Sohrabi, M.J.; Mirzadeh, H. Interdiffusion coefficients of alloying elements in a typical Ni-based superalloy. *Vacuum* **2019**, *169*, 108875. [\[CrossRef\]](#)
16. Schneider, M.C.; Gu, J.P.; Beckermann, C.; Boettinger, W.J.; Kattner, U.R. Modeling of micro- and macrosegregation and freckle formation in single-crystal nickel-base superalloy directional solidification. *Met. Mater. Trans. A* **1997**, *28*, 1517–1531. [\[CrossRef\]](#)
17. Wang, Y.; Tan, Y.; Li, X.; Zhao, J.; You, X. Microsegregation and homogenization behavior of a Ni-Co based refractory superalloy for turbine discs. *Mater. Charact.* **2023**, *196*, 112598. [\[CrossRef\]](#)
18. Karunaratne, M.; Cox, D.; Carter, P.; Reed, R. Modelling of the Microsegregation in CMSX-4 Superalloy and its Homogenisation During Heat Treatment. *Superalloys 2000*, *2000*, 263–272. [\[CrossRef\]](#)
19. Bokstein, B.; Epishin, A.; Link, T.; Esin, V.; Rodin, A.; Svetlov, I. Model for the porosity growth in single-crystal nickel-base superalloys during homogenization. *Scr. Mater.* **2007**, *57*, 801–804. [\[CrossRef\]](#)
20. Zhang, H.; Wang, Y.; De Vecchis, R.R.; Xiong, W. Evolution of Carbide Precipitates in Haynes@282 Superalloy Processed by Wire Arc Additive Manufacturing. *J. Mater. Process. Technol.* **2022**, *305*, 117597. [\[CrossRef\]](#)
21. Tin, S.; Pollock, T.M.; King, W.T. Carbon Additions and Grain Defect Formation in High Refractory Nickel-Base Single Crystal Superalloys. In Proceedings of the Superalloys 2000, Ninth International Symposium, TMS, Seven Springs, PA, USA, 17–21 September 2000; pp. 201–210. [\[CrossRef\]](#)
22. Li, Q.; Xie, J.; Yu, J.; Shu, D.; Hou, G.; Sun, X.; Zhou, Y. Solidification behavior and segregation characteristics of high W-content cast Ni-Based superalloy K416B. *J. Alloys Compd.* **2021**, *854*, 156027. [\[CrossRef\]](#)
23. Wang, Y.; Sun, F.; Dong, X.; Zhang, L.; Shan, A. Thermodynamic study on equilibrium precipitation phases in a novel Ni-Co base superalloy. *Acta Metall. Sin.* **2010**, *46*, 334–339. [\[CrossRef\]](#)

24. Xu, Y.; Jin, Q.; Xiao, X.; Cao, X.; Jia, G.; Zhu, Y.; Yin, H. Strengthening mechanisms of carbon in modified nickel-based superalloy Nimonic 80A. *Mater. Sci. Eng. A* **2011**, *528*, 4600–4607. [[CrossRef](#)]
25. Lvov, G.; Levit, V.I.; Kaufman, M.J. Mechanism of Primary MC Carbide Decomposition in Ni-Base Superalloys. *Metall. Mater. Trans. A* **2004**, *35*, 1669–1679. [[CrossRef](#)]
26. Qin, X.Z.; Guo, J.T.; Yuan, C.; Hou, J.S.; Ye, H.Q. Precipitation and Thermal Instability of M<sub>23</sub>C<sub>6</sub> Carbide in Cast Ni-Base Superalloy K452. *Mater. Lett.* **2008**, *62*, 258–261. [[CrossRef](#)]
27. Ebrahimian, M.; Rizi, M.S.; Hong, S.I.; Kim, J.H. Effects of Molybdenum on Hot Deformation Behavior and Microstructural Evolution of Fe<sub>40</sub>Mn<sub>40</sub>Co<sub>10</sub>Cr<sub>10</sub>C<sub>0.5</sub> High Entropy Alloys. *Sci. Technol. Adv. Mater.* **2023**, *24*, 2186119. [[CrossRef](#)]
28. Rizi, M.S.; Minouei, H.; Lee, B.J.; Pouraliakbar, H.; Toroghinejad, M.R.; Hong, S.I. Hierarchically activated deformation mechanisms to form ultra-fine grain microstructure in carbon containing FeMnCoCr twinning induced plasticity high entropy alloy. *Mater. Sci. Eng. A* **2021**, *824*, 141803. [[CrossRef](#)]
29. Zhao, G.-D.; Zang, X.-M.; Sun, W.-R. Role of carbon in modifying solidification and microstructure of a Ni-based superalloy with high Al and Ti contents. *J. Iron Steel Res. Int.* **2021**, *28*, 98–110. [[CrossRef](#)]
30. Wei, C.-N.; Bor, H.-Y.; Chang, L. The effects of carbon content on the microstructure and elevated temperature tensile strength of a nickel-base superalloy. *Mater. Sci. Eng. A* **2010**, *527*, 3741–3747. [[CrossRef](#)]
31. Xu, H.; Zhang, Y.; Fu, H.; Xue, F.; Zhou, X.; Xie, J. Effects of boron or carbon on solidification behavior of Co-Ni-Al-W-based superalloys. *J. Alloys Compd.* **2022**, *891*, 161965. [[CrossRef](#)]
32. Lukas, H.; Fries, S.G.; Sundman, B. *Computational Thermodynamics*; Cambridge University Press: Cambridge, UK, 2007. [[CrossRef](#)]
33. Wu, J.; Meng, J.; Zou, M.; Yao, L.; Wang, X.; Yang, Y.; Zhou, Y.; Sun, X. Effect of wall thickness on micropores and stress-rupture properties of a single-crystal nickel-based superalloy. *Mater. Sci. Eng. A* **2023**, *872*, 144941. [[CrossRef](#)]
34. Huang, Z.; He, X.; Chen, K.; Wang, X. Solidification and segregation characteristics of Ni-based superalloy C700R-1 for ultra-supercritical steam turbine rotor. *J. Alloys Compd.* **2022**, *912*, 165107. [[CrossRef](#)]
35. Campbell, C.; Boettinger, W.; Kattner, U. Development of a diffusion mobility database for Ni-base superalloys. *Acta Mater.* **2002**, *50*, 775–792. [[CrossRef](#)]
36. Warnken, N.; Ma, D.; Drevermann, A.; Reed, R.; Fries, S.; Steinbach, I. Phase-field modelling of as-cast microstructure evolution in nickel-based superalloys. *Acta Mater.* **2009**, *57*, 5862–5875. [[CrossRef](#)]
37. Gasson, P.C. *The Superalloys: Fundamentals and Applications* R. C. Reed Cambridge University Press, The Edinburgh Building, Shaftesbury Road, Cambridge, CB2 2RU, UK, 2006. 372pp. Illustrated. £80. ISBN 0-521-85904-2. *Aeronaut. J.* **2008**, *112*, 291. [[CrossRef](#)]
38. Epishin, A.; Link, T.; Svetlov, I.L.; Nolze, G.; Neumann, R.S.; Lucas, H. Mechanism of porosity growth during homogenisation in single crystal nickel-based superalloys. *Int. J. Mater. Res.* **2013**, *104*, 776–782. [[CrossRef](#)]
39. Anton, D.; Giamei, A. Porosity distribution and growth during homogenization in single crystals of a nickel-base superalloy. *Mater. Sci. Eng.* **1985**, *76*, 173–180. [[CrossRef](#)]
40. Li, X.; Wang, L.; Dong, J.; Lou, L. Effect of Solidification Condition and Carbon Content on the Morphology of MC Carbide in Directionally Solidified Nickel-base Superalloys. *J. Mater. Sci. Technol.* **2014**, *30*, 1296–1300. [[CrossRef](#)]
41. Banaszek, G.; Stefanik, A. Theoretical and laboratory modelling of the closure of metallurgical defects during forming of a forging. *J. Am. Acad. Dermatol.* **2006**, *177*, 238–242. [[CrossRef](#)]

**Disclaimer/Publisher’s Note:** The statements, opinions and data contained in all publications are solely those of the individual author(s) and contributor(s) and not of MDPI and/or the editor(s). MDPI and/or the editor(s) disclaim responsibility for any injury to people or property resulting from any ideas, methods, instructions or products referred to in the content.